Inorganic Chemistry

Article

Cite This: Inorg. Chem. 2018, 57, 10341−10351

pubs.acs.org/IC

High-Pressure Synthesis of β-Ir_4B_5 and Determination of the Compressibility of Various Iridium Borides

Benedikt Petermüller,[†] Christopher Neun,[‡] Klaus Wurst,[†] Lkhamsuren Bayarjargal,[‡] Dominik Zimmer,[‡] Wolfgang Morgenroth,[‡] Miguel Avalos-Borja,[§] Ignacio Guadalupe Becerril-Juarez,[§] Martin J. Mühlbauer,[∥,⊥] Björn Winkler,[‡] and Hubert Huppertz*[,†]

[†]Institut für Allgemeine, Anorganische und Theoretische Chemie, Leopold-Franzens-Universität Innsbruck, Innrain 80-82, 6020 Innsbruck, Austria

[‡]Institut für Geowissenschaften, Abteilung für Kristallographie, Goethe-Universität Frankfurt am Main, Altenhöferallee 1, 60438 Frankfurt, Germany

[§]Instituto Potosino de Investigacion Cientifica y Tecnologica, Division de Materiales Avanzados, San Luis Potosi 78216, Mexico

[∥]Heinz Maier-Leibnitz Zentrum (MLZ), Technische Universität München, Lichtenbergstr. 1, 85748 Garching, Germany

[⊥]Institute for Applied Materials (IAM), Karlsruhe Institute of Technology (KIT), Hermann-von-Helmholtz-Platz 1, 76344 Eggenstein-Leopoldshafen, Germany

Supporting Information

ABSTRACT: A new iridium boride, β-Ir_4B_5, was synthesized under high-pressure/high-temperature conditions of 10.5 GPa and 1500 °C in a multianvil press with a Walker-type module. The new modification β-Ir_4B_5 crystallizes in a new structure type in the orthorhombic space group *Pnma* (no. 62) with the lattice parameters a = 10.772(2) Å, b = 2.844(1) Å, and c = 6.052(2) Å with $R1$ = 0.0286, $wR2$ = 0.0642 (all data), and Z = 2. The structure was determined by single-crystal X-ray and neutron powder diffraction on samples enriched in ^{11}B. The compound is built up by an alternating stacking of boron and iridium layers with the sequence ABA′B′. Additionally, microcalorimetry, hardness, and compressibility measurements of the binary iridium borides α-Ir_4B_5, β-Ir_4B_5, Ir_5B_4, hexagonal Ir_4B_{3-x} and orthorhombic Ir_4B_{3-x} were carried out and theoretical investigations based on density function theory (DFT) were employed to complement a comprehensive evaluation of structure−property relations. The incorporation of boron into the structures does not enhance the compressibility but leads to a significant reduction of the bulk moduli and elastic constants in comparison to elemental iridium.

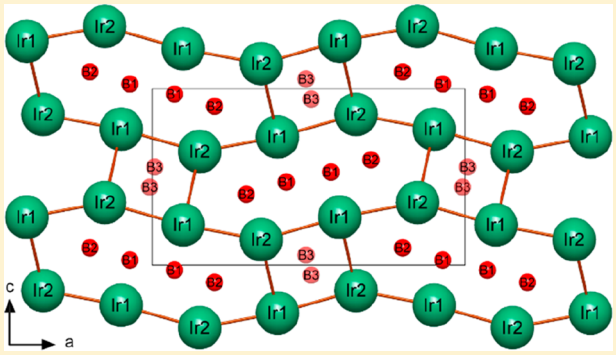

INTRODUCTION

Over the past few years, metal borides attracted major interest within the scientific community, as many of them have outstanding physical properties, such as a high hardness (ReB_2, WB_4, FeB_4, $IrB_{1.35}$[1−4]), extremely low compressibilities (ReB_2, OsB[1,5]), superconductivity (MgB_2, NbRuB[6,7]), and outstanding high melting points (ZrB_2, HfB_2[8]). As a result of their high thermal stabilities, borides are often used in high temperature applications.[9] Most borides can be synthesized at ambient pressure, which makes these materials interesting for industrial applications, as this synthesis route is relatively inexpensive and easily accessible.[1,3,4,8−10]

In contrast to the limited experimental work on borides synthesized under high-pressure conditions, various theoretical studies predicted the possible synthesis of FeB_4, ReB_4, TaB_4, IrB_2, and IrB_4, among others, under high-pressure conditions.[11−14] Specifically, the existence of a new iron-tetraboride FeB_4 with interesting physical properties like outstanding hardness and superconductivity was originally predicted by Kolmogorov et al.[15] and Bialon et al.,[16] who suggested that FeB_4 could be synthesized under high-pressure conditions. In 2014, Gou et al. successfully synthesized FeB_4 under high-pressure conditions at a pressure of 15 GPa and a temperature of 1573 K.[2] Later on, the predicted orthorhombic structure as well as the superconductivity of FeB_4 were confirmed by experiment.[2,15,16] In addition to FeB_4, only very few further borides such as, e.g., Fe_2B_7, MnB_4, Co_3B_{16}, and CrB_4 were synthesized under high-pressure conditions.[2,17−24]

In order to expand the available limited data, the focus in this work is the synthesis of new iridium borides under high-pressure conditions. Up to now, already six binary iridium borides are known, namely, Ir_4B_{5+x} (formerly $IrB_{1.35}$),[10,25−27] Ir_5B_{4+x} (formerly $IrB_{1.1}$),[10,25,26] and the high and low

Received: June 6, 2018
Published: August 7, 2018

DOI: 10.1021/acs.inorgchem.8b01541
Inorg. Chem. 2018, 57, 10341−10351

temperature modification of Ir_4B_{3-x} (formerly $IrB_{0.9}$).[10,28] These phases were synthesized via high temperature syntheses by Aronsson et al.[25,26] and by Rogl et al.[28] More recently, Zeiringer et al. reinvestigated the chemical compositions and structures of these iridium borides and suggested a slightly different labeling for a more suitable specification of the phase width.[10] In 2016, Xie et al. successfully used a mechanochemical approach to synthesize two new iridium borides, namely, IrB_2 and IrB.[29] Rau et al. and Latini et al. investigated the hardness of Ir_4B_{5+x} (formerly $IrB_{1.35}$) and Ir_5B_{4+x} (formerly $IrB_{1.1}$) and discovered that very thin films of both phases show a high hardness of 49.8 at a load of 0.49 N for Ir_4B_{5+x} and 43 GPa at 0.49 for Ir_5B_{4+x}.[3,30] With the exception of the hardness of those phases, very little is known about other properties, such as compressibility, of the iridium borides. Numerous predictions of novel iridium borides with varying Ir:B ratio, which possibly could be synthesized under high-pressure/high-temperature conditions and are expected to show interesting mechanical properties, have been made.[10,12−14,31−34]

In this context, our experiments led to the successful synthesis of a new modification of Ir_4B_5 which crystallizes in the centrosymmetric space group *Pnma* in a new crystal structure type. Due to the extremely low scattering cross section of boron in comparison with iridium for X-rays, it is practically impossible to reliably determine the exact position and occupation of the boron atoms solely on the basis of X-ray diffraction data. Therefore, neutron powder diffraction data on ^{11}B-enriched samples were used in combination with X-ray diffraction methods to determine the structure. In addition to the synthesis of the new modification, we examined the compressibility, hardness, and thermodynamical properties of various other iridium borides.

EXPERIMENTAL SECTION

Synthesis. The starting materials iridium (99.9+%, ChemPur, Karlsruhe, Germany) and amorphous boron (99.9+%, ChemPur, Karlsruhe, Germany) or crystalline ^{11}B (99.9+% purity, 99.8+% enrichment, Ceradyne 3M, St. Paul, USA) were used for all phases. For the synthesis of β-Ir_4B_5, a stoichiometric Ir:B ratio of 1:3 was used. Experiments with a Ir:B ratio of 1:1.2 did not lead to the synthesis of β-Ir_4B_5 and showed that some excess of boron is necessary for the successful synthesis. The mixture was ground in a ball mill (Pulverisette 7-Premium Line, Fritsch, Idar-Oberstein, Germany) with an internal bowl volume of 80 mL for 100 min. Seven tungsten carbide balls were used as milling media with a ball to powder weight ratio of 1:15. Afterwards, the powder was inserted into a crucible made from hexagonal boron nitride (HeBoSint P100, Henze BNP GmbH, Kempten, Germany) and inserted into a 14/8 assembly. The sample was compressed to 10.5 GPa within 4.5 h by a high-pressure device consisting of a hydraulic 1000 t press (mavo press LPR 1000-400/50, Max Voggenreiter GmbH, Mainleus, Germany) and a Walker-type module (Max Voggenreiter GmbH) with eight tungsten carbide cubes (HA-7% Co, Hawedia, Marklkofen, Germany). The mixture was heated from ambient temperature to 1500 °C within 5 min. The temperature was held for 30 min and afterwards reduced to 700 °C in 1 h. After decompression, the sample was isolated from the surrounding assembly parts by mechanical separation. A more detailed description of this setup can be found in the literature.[35,36]

Samples of α-Ir_4B_5 were synthesized in an arc melter (MAM-1, E. Bühler GmbH, Hechingen, Germany) by annealing the elements in an Ir:B ratio of 1:1.5. The powders were mixed in an agate mortar and pressed into pellets of 5 mm diameter. Prior to the experiment, a titanium getter (99.95%) was molten to absorb any remaining traces of oxygen from the atmosphere in the reaction chamber. During the synthesis, the pellet was not molten but annealed by the plasma several times from different sides. The temperature could thus not be determined exactly but must have been close to the melting point at the sample surface. A temperature gradient from the surface to the bulk must be assumed.

Samples of Ir_5B_4 could be synthesized in a custom-built tube furnace from the elements at 1223 K. The starting materials were mixed in an agate mortar in a Ir:B ratio of 1.25:1 and pressed into a dense pellet of 5 mm in diameter. The pellet was placed in a ceramic crucible and heated to 1223 K. The temperature was held for 24 h before switching the furnace off. The analysis of the powder X-ray diffraction pattern of Ir_5B_4 revealed that no side phases were present after the synthesis. The orthorhombic and hexagonal modifications of Ir_4B_{3-x} were synthesized simultaneously from the same pellet. This was achieved by annealing the compacted powder with the plasma beam at low powers, which did not suffice to melt the elements. Since the phase transformation takes place at moderate temperatures (1373−1473 K), the temperature gradient from the surface to the bulk of the pellet in this method enabled us to obtain both modifications at once.

Crystal Structure Determination. The powder X-ray diffraction pattern of β-Ir_4B_5 was obtained in transmission geometry from a flat powder sample of the product. The measurements were carried out in transmission geometry using a STOE STADI P powder diffractometer equipped with Mo-$K_{\alpha1}$-radiation (Ge(111) monochromator λ = 0.7093 Å) in the 2θ range of 2.0−90.2° with a step size of 0.015°. As a detector, a silicon microstrip solid state detector (Dectris Mythen 1K) was used. The lattice parameters shown in Table 1 were obtained through a Rietveld analysis of the powder pattern using the program TOPAS.[37] The Rietveld analysis of the powder pattern (Figure 1) revealed a very weak amorphous halo which can be explained by some unreacted amorphous boron, some weak reflections (e.g., at 10.9, 16.9, and 23.0°) which can be assigned to the compound IrB_2 (ReB_2-type), and a few additional reflections (12.1, 12.7, and 18.2°) which could not yet be assigned to any known phase and presumably belong to an unknown minor impurity phase.

Small single-crystals of β-Ir_4B_5 were selected by mechanical fragmentation using a polarization microscope. A Bruker D8 Quest Kappa diffractometer with Mo-K_α radiation (λ = 0.71073 Å) was used to collect the single-crystal intensity data at room temperature. A multiscan absorption correction (SADABS-2014[38]) was applied to the intensity data sets. The structure solution and parameter refinement (full matrix least squares against F^2) were performed by using the SHELX-13 suite with anisotropic displacement parameters for all atoms.[39,40] To ensure that no symmetry operations were missing, the final solution was checked with PLATON.[41] All relevant details of the data collection and the refinement are listed in Table 1, the positional parameters are listed in Table 2, and the important bond lengths are listed in Table 3. The program Diamond was used for the graphical representation (Figures 2−7) of the structure.[42]

Neutron Powder Diffraction. Neutron powder diffraction was carried out at the neutron source FRM II at the Heinz Maier-Leibnitz Zentrum (MLZ), Garching, Germany, using the high-resolution neutron powder diffractometer SPODI with a Ge(551) monochromator (λ = 1.5481 Å). The data were collected in a range of 160° by a bank consisting of 80 ^3He detector tubes. A detailed description of the high-resolution neutron powder diffractometer can be found in the literature.[43,44] Due to the high absorption cross sections of B and Ir, the samples were placed in a glass capillary with a diameter of only 1 mm for the measurement and measured for 90 min. The probe exhibits a packing density of around 2.39 g/cm^3 within the capillary. The packing density in combination with the atomic scattering factors of the used elements and the absorption leads to an attenuation factor for the sample of 2.546 cm^{-1}, which was used during the Rietveld refinement.[45,46] The Rietveld refinement was carried out using the program TOPAS[37] and was used to determine the boron positions and occupancy. Due to the complicated synthesis process, the sample, which was used for the neutron diffraction, was relatively small and therefore the ratio of peak intensity to background was rather weak. The analysis of the neutron data, however, could unambiguously

DOI: 10.1021/acs.inorgchem.8b01541
Inorg. Chem. 2018, 57, 10341−10351

Table 1. Crystal Data and Structure Refinement of β-Ir_4B_5 (Standard Deviations in Parentheses)

empirical formula	β-Ir_4B_5
molar mass, g·mol^{-1}	822.86
crystal system	orthorhombic
space group	*Pnma* (no. 62)
Powder Data	
powder diffractometer	STOE Stadi P
radiation	Mo-$K_{\alpha 1}$ (λ = 0.7093 Å)
a, Å	10.758(2)
b, Å	2.837(2)
c, Å	6.038(3)
V, Å^3	184.32(4)
Single-Crystal Data	
single-crystal diffractometer	Bruker D8 Quest Kappa
radiation	Mo-K_α (λ = 0.71073 Å)
a, Å	10.772(2)
b, Å	2.844(1)
c, Å	6.052(2)
V, Å^3	185.47(2)
formula units per cell, *Z*	2
calculated density, g cm^{-3}	14.73
crystal size, mm^3	0.050 × 0.045 × 0.040
temperature, K	292(2)
absorption coefficient, mm^{-1}	142.8
F(000)	666
θ range, deg	3.8−39.9
range in *hkl*	$-19 \le h \le 19$, $-5 \le k \le 5$, $-9 \le l \le 10$
total no. of reflections	7081
independent reflections	651
reflections with $I \ge 2\sigma(I)$	624
data/parameters	651/32
absorption correction	multiscan
goodness-of-fit on F^2	1.262
final *R* indices [$I \ge 2\sigma(I)$]	*R*1 = 0.0271
	*w*R2 = 0.0635
final *R* indices (all data)	*R*1 = 0.0286
	*w*R2 = 0.0642
largest diff. peak and hole, e Å^{-3}	5.07/−3.76

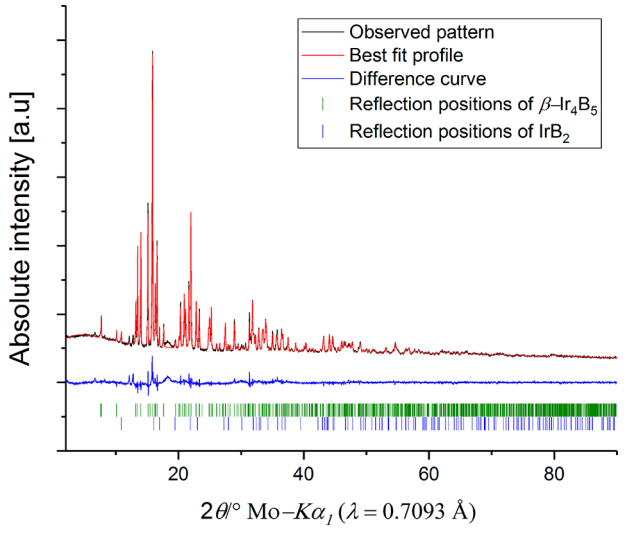

Figure 1. Rietveld plot of β-Ir_4B_5. The experimental powder diffraction pattern is shown in black, the calculated pattern is shown in red, and the difference plot is shown in blue. The reflection positions of β-Ir_4B_5 are shown in green, and those of IrB_2, in blue.

Table 2. Atomic Coordinates (Wyckoff Position 4*c* for All Atoms) and Equivalent Anisotropic Displacement Parameters U_{eq} (Å^2) of β-Ir_4B_5[a]

atom	*x*	*y*	*z*	U_{eq}[b]	s.o.f.
Ir1	0.59904(3)	1/4	0.2719(5)	0.0057(2)	1
Ir2	0.84838(3)	1/4	0.3555(5)	0.0055(2)	1
B1	0.5713(9)	3/4	0.528(2)	0.007(2)	1
B2	0.801(2)	3/4	0.097(2)	0.008(2)	1
B3	0.008(2)	1/4	0.557(3)	0.007(3)	0.5

[a]Data collected by single-crystal X-ray diffraction. [b]U_{eq} is defined as one-third of the trace of the orthogonalized U_{ij} tensor.

Table 3. Interatomic Distances (Å) in β-Ir_4B_5 (Space Group *Pnma*), Derived from Single-Crystal Data

2 × Ir1−B1	2.128(8)	Ir2−B1	2.16(2)
Ir1−B1	2.20(2)	2 × Ir2−B2	2.172(7)
Ir1−B2	2.25(2)	Ir2−B2	2.18(2)
Ir1−B3	2.22(2)	2 × Ir2−B3	2.17(2)
2 × Ir1−B3	2.25(2)	Ir2−B3	2.11(2)
2 × Ir1−Ir1	2.8445(2)	Ir2−Ir1	2.9489(4)
Ir1−Ir2	2.9489(4)	Ir2−Ir1	2.8082(5)
Ir1−Ir2	2.7332(5)	2 × Ir2−Ir2	2.8445(2)
Ir1−Ir2	2.8082(5)		
4 × B1−B2	2.02(2)	2 × B3−B3	1.59(2)
2 × B1−B1	2.12(2)		

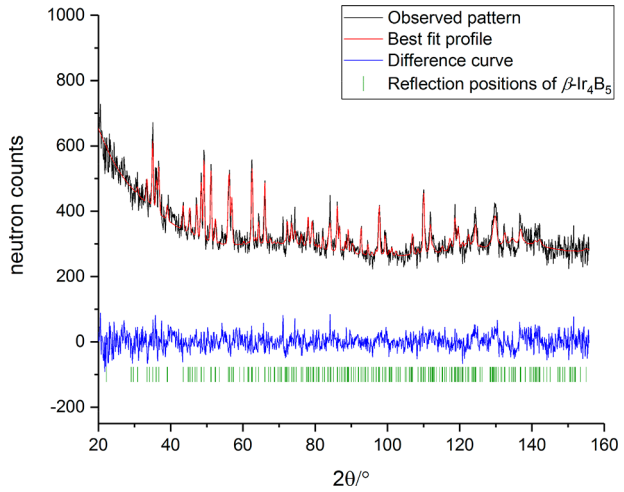

Figure 2. Rietveld plot of β-Ir_4B_5 derived from the neutron data. The experimental powder diffraction pattern is shown in black, the calculated pattern is shown in red, and the difference plot is shown in blue.

verify the results of the X-ray structure determination (Figures 1 and 2, Supporting Information Tables S1 and S2).

Further details of the crystal structure investigation may be obtained from the Fachinformationszentrum Karlsruhe, D-76344 Eggenstein-Leopoldshafen, Germany (fax: +49-7247-808-666; e-mail: crysdata@fiz-karlsruhe.de, http://www.fiz-karlsruhe.de/request) on quoting the deposition number CSD-433663.

Determination of the Compressibility. For high-pressure experiments, Boehler-Almax-type diamond anvil cells were used.[47] The cells were loaded with Ne as a pressure-transmitting medium. Samples were placed in holes of 110−130 μm in diameter, which were drilled by a custom-built laser lathe in preindented Re gaskets (40−50 μm in thickness). The pressure was determined using the ruby fluorescence method.[48] Synchrotron X-ray diffraction experiments at high pressures were performed at the beamline P02.2 of the PETRA

DOI: 10.1021/acs.inorgchem.8b01541
Inorg. Chem. 2018, 57, 10341−10351

III synchrotron (DESY, Hamburg, Germany). The diffraction patterns were acquired with a PerkinElmer XRD1621 detector at a wavelength of 0.2902 Å with beams focused to 1.5 × 2.3 μm fwhm by Kirkpatrick–Baez mirrors. In order to improve the sampling statistics, samples were rotated by 20° during the 10 s data acquisition time. A CeO_2 standard was used to determine the sample-to-detector distance and for detector calibration during the experiments.[49] The diffraction patterns were corrected and integrated using the FIT2D and DIOPTAS software packages.[50,51] The compressibilities were determined by investigating the dependence of the unit cell parameters upon compression which were obtained by Le Bail refinements. The data were fitted using a third-order Birch–Murnaghan (BM) equation of state[52,53] using the EosFit software package.[54]

Microcalorimetry. Microcalorimetry was performed using a Quantum Design thermal relaxation calorimeter (Physical Properties Measurement System, Quantum Design, San Diego, USA). Powdered samples of boron were thoroughly ground in a tungsten carbide mortar to reduce pores and encapsulated in a copper container (Alfa Aesar, 99.999%). In this case, the heat capacity of copper had to be subtracted afterward. Compacted, polycrystalline fragments of samples from α-Ir_4B_5, β-Ir_4B_5, and iridium were prepared so that one flat and polished surface was present to guarantee a good thermal coupling of the sample to the sample holder. We have shown the accuracy of our measurements to be 1% in the temperature region between 40 and 300 K and 2% below 40 K by comparing the measurement of a standard material (Cu, Alfa Aesar, 99.999%) with the values obtained by Lashley et al.[55] The samples were mounted using Apiezon-N grease. All samples weighed between 10 and 25 mg and were measured in the temperature range between 1.8 and 395 K at 150 different temperatures. The temperature steps were reduced logarithmically from 395 to 1.8 K. At each step, the heat capacity was measured three times by the relaxation method using the two-τ model.[55−57]

Hardness Measurements. Hardness measurements were carried out using a Vickers-type microhardness testing machine (HM-210A, Mitutoyo, Japan), equipped with an optical microscope and a 50× lens. A standard square-based diamond pyramid indenter with a 136° apex angle between the opposite faces was used for the indentation. Every indentation spot was generated by applying the following conditions: The loading and unloading times were kept at 5 s before and after the retention time of 15 s. The approaching speed of the indenter was 60 μm/s. We created 10 indentations on the sample surface at each testing load (0.49, 0.98, 1.96, 2.94, 4.9, and 9.8 N). The Vickers hardness (H_V) was derived using the equation

$$H_V = \frac{1}{g}\frac{2F\sin\frac{136^\circ}{2}}{d^2}$$

with g being the standard gravitational acceleration (m/s^2), F the indentation load (N), and d the average diagonal imprint distance (mm). For the conversion to GPa, the results were multiplied by the factor 0.009807.

To provide an optimal specimen with a parallel surface for the hardness measurements, five polycrystalline fragments of β-Ir_4B_5 were embedded in a high-yield two-component epoxy (UHU Endfest 300, UHU, Brühl, Germany) inside a customized brass ring (5 mm in height, 20 mm in diameter). The entire setup was grounded using diamond coated polishing disks of varying mesh sizes, and the error in parallelism was ±2 μm. The top side, on which we carried out the measurements, was polished to a mirror-like finish using Al_2O_3 powder with grain sizes of 1 and 3 μm.

Density Functional Theory. In order to obtain a better understanding of the structure–property relations of the synthesized compounds, we performed density functional theory (DFT) calculations employing the CASTEP[58] code. This code implements the Kohn–Sham DFT based on a plane wave basis set in conjunction with pseudopotentials. The plane wave basis set is unbiased (as it is not atom-centered) and does not suffer from basis set superposition errors in comparison to atom-centered analogues. It also makes converged results straightforward to obtain in practice, as the convergence is controlled by a single adjustable parameter, the plane wave cutoff, which was set to 390 eV. All pseudopotentials were ultrasoft and were generated using the WC-GGA to allow for a fully consistent treatment of the core and valence electrons.[59] Brillouin zone integrals were performed by using Monkhorst–Pack grids with spacings of less than 0.028 Å^{-1} between individual grid points. A simultaneous optimization of the unit cell parameters and internal coordinates was performed in the way that forces were converged to <0.005 eV/Å and the stress residual was <0.005 GPa. Elastic stiffness coefficients were derived by stress–strain calculations.

RESULTS AND DISCUSSION

Crystal Structure of β-Ir_4B_5. According to the systematic extinctions, the orthorhombic space group *Pnma* (no. 62) was derived for β-Ir_4B_5. The dimensions of the unit cell are a = 10.772(2) Å, b = 2.844(1) Å, c = 6.052(2) Å, and V = 185.47(2) Å^3 (Table 1). The crystal structure was solved via single-crystal X-ray diffraction, but as it is difficult to reliably determine the occupancy and exact positions of the boron atoms solely on the basis of X-ray diffraction data, neutron powder diffraction was carried out afterward to verify the structure solution (Figures 1 and 2). Unless otherwise stated, the crystallographic details used in the following discussion (bond lengths and angles) are based on the excellent single-crystal X-ray data, as the quality of the powder pattern obtained from the neutron diffraction data was too low to deviate exact values from it (Figures 1 and 2, Tables 1 and S2). Nevertheless, the neutron diffraction data generally confirmed the single-crystal X-ray data. Furthermore, the investigations show that β-Ir_4B_5 possesses a phase width and could therefore be labeled as β-$Ir_4B_{5\pm x}$, as Zeiringer et al. also suggested for other iridium borides.[10] However, in the following, we use the idealized formula β-Ir_4B_5. Figure 3 shows the structure, which

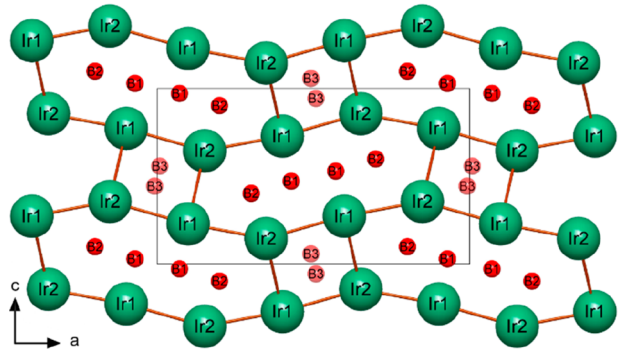

Figure 3. Stacking of alternating puckered boron (red) layers and puckered iridium atoms (light green).

can be described as stacking of alternating puckered boron layers (B, B′) and puckered iridium layers (A, A′) in the stacking sequence ABA′B′ in the c direction of the crystal structure. The boron layers are built up by two parallel boron chains consisting of B1 and B2 atoms. These chains are interconnected via the B1 atoms of each chain, leading to the formation of a unique ribbonlike network of boron atoms (Figure 4). The boron–boron distances within the ribbons are 2.024(10) Å for B1–B1 and 2.122(14) Å for B1–B2 and are thus relatively long, but they correspond well to boron–boron distances in other transition-metal borides.[10,17,25,60] These ribbons are located within large cavities formed by eight iridium atoms (Figure 3). Between the boron ribbons of each

DOI: 10.1021/acs.inorgchem.8b01541
Inorg. Chem. 2018, 57, 10341−10351

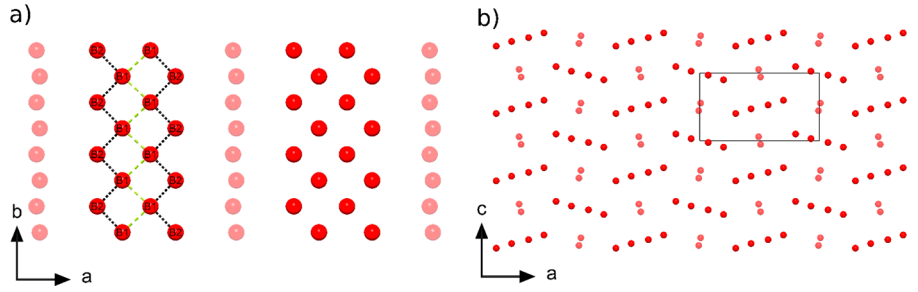

Figure 4. (a) Projection of a boron layer consisting of interconnected (green bonds) zigzag chains (black bonds) forming ribbons. Between the ribbons, half-occupied slightly bent boron chains (light red) are located. (b) Puckered boron layers along [010].

individual layer, iridium atoms form a column of face-sharing trigonal prisms that are partly centered by boron atoms B3. These prisms are connected via the square faces building up a column in the *b* direction (Figure 5). The structure

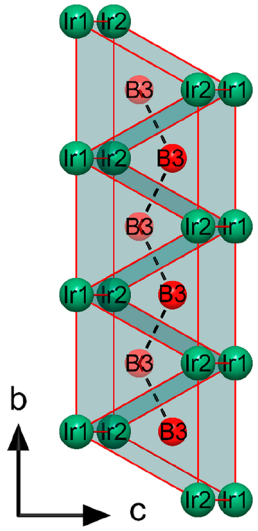

Figure 5. Column of face-sharing Ir_6 prisms centered by a half-occupied boron chain.

determination based on X-ray data revealed an occupancy of ~50% for B3 in the centers of the prisms within the column. The neutron data were used to verify the occupancy of around 50% for the B3 position and revealed a site occupancy factor of 55(4)%. The result of the neutron data is congruent with the X-ray data and is reasonable regarding the fact that a full occupancy of the prisms would lead to the formation of a boron chain with a very short boron−boron distance of just 1.589(18) Å (Tables 2 and 3). As the B3 position exhibits an occupancy of marginally above 50%, some chain fragments with very short boron−boron distances may exist within the structure. The B3 positions are slightly shifted from being aligned in a perfectly straight chain (Figure 5). As the analysis of the X-ray data did not show any superstructure reflections, we cannot assume an ordering on the B3 site. The alignment within the individual boron layers (B and B′) is identical, but the different layers are rotated and shifted with respect to each other (Figure 4b). The iridium atoms form a framework with two types of cavities, which are occupied by either the boron ribbons (B1 and B2) or the "chain" of isolated boron atoms (B3) (Figure 3). Iridium−iridium distances in the framework range from 2.7332(5) to 2.9489(4) Å, which is similar to the iridium−iridium distances in other borides and metallic iridium.[10,26,28,61,62] Whereas the boron atoms B2 at the edge of the ribbons are coordinated by four iridium and two boron atoms, the boron atoms B1 have four close boron neighbors and four iridium atoms, leading to an 8-fold coordination (4 Ir + 4 B). The bond lengths of Ir−B within the iridium cage range from 2.128(8) to 2.249(11) Å and within the trigonal prism from 2.108(19) to 2.249(11) Å, which is slightly shorter than the sum (2.25 Å) of the covalent radii of the B atom (r = 0.84 Å) and the Ir atom (r = 1.41 Å). The iridium atoms are coordinated by six iridium atoms as well as by seven boron atoms, leading to a 13-fold coordination.

The closely related α-modification of Ir_4B_{5+x} can be synthesized by arc melting and crystallizes in the monoclinic space group $C2/m$ with a = 10.520(1) Å, b = 2.895(1) Å, c =

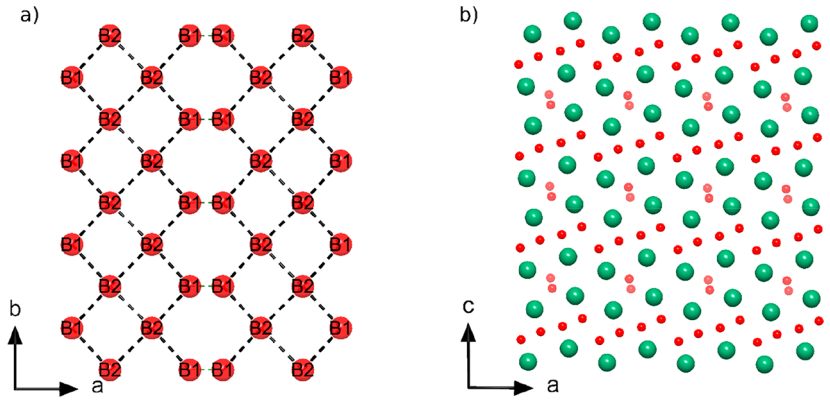

Figure 6. (a) Boron layer in α-Ir_4B_5 viewed along $[00\bar{1}]$ exhibiting the boron network with shorter (green) and longer (black) boron−boron bonds. (b) Layered structure of α-Ir_4B_5 consisting of boron layers and double iridium layers with boron atoms in the interstices.[10,25,27]

DOI: 10.1021/acs.inorgchem.8b01541
Inorg. Chem. 2018, 57, 10341−10351

6.095(1) Å, β = 91.156(2)°, and V = 185.6 Å^3.[10,25,27,60] Just like β-Ir_4B_5, α-Ir_4B_5 can also be described by a stacking of puckered boron and puckered double metal layers, however, without any displacements of the layers, therefore leading to the simple stacking sequence ABAB (Figure 6b). The interstices of the metal double layers are filled with boron atoms forming boron chains with rather short B−B distances of 1.61 Å. The boron atoms have a trigonal prismatic environment of iridium atoms, and the structure determination also revealed an occupancy of 50% for these boron positions.[10] The same structural motif can be found in β-Ir_4B_5, but in contrast to the β-modification, these boron chains in the α-modification are located within the iridium layers and are not part of the boron layers (Figures 4, 6, and 7). Boron atoms with a trigonal prismatic metal environment are very common and can be found within several other transition metal borides such as Re_3B, Ni_7B_3, and the members of the AlB_2 and CrB structure type family.[63−66] In contrast to the arrangement of isolated boron ribbons in β-Ir_4B_5, the boron atoms within α-Ir_4B_5 form an infinite boron network with B−B distances of 1.877 Å between B1 and B1 and 2.106 Å between B2 and B2 (Figure 6).[10,25−27,60]

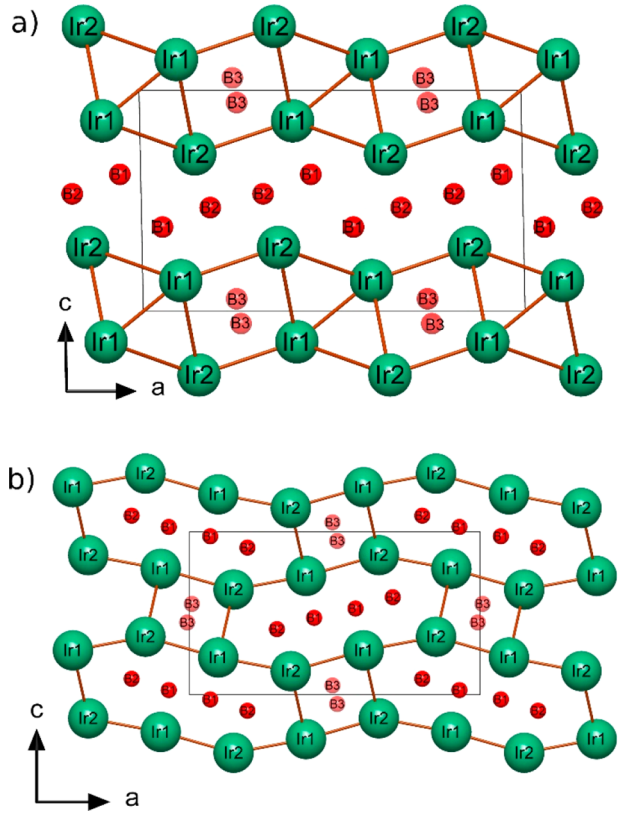

Figure 7. Structures of (a) α-Ir_4B_5 and (b) β-Ir_4B_5.

Similar infinite two-dimensional boron networks can also be found within many other borides with a metal vs boron ratio ranging from MB_2 to M_2B_5.[27,61,65,67] The existence of interconnected and isolated boron chains within the same phase, as has been observed here in β-Ir_4B_5, has only been found in borides possessing the V_5B_6-structure type. In V_5B_6, the double chain consists of two antiparallel boron chains that are interconnected. The connection of the two chains leads to the formation of a boron network, which can also be described as a chain of aligned B_6 hexagons (Figure 8).[68,69]

Compressibility. In the pressure regime up to 38 GPa, α-Ir_4B_5 shows no structural phase transition. The bulk modulus is B_0 (α-Ir_4B_5, third order) = 280(6) GPa with the pressure derivative B' (α-Ir_4B_5, third order) = 4.4(4). The lattice parameters show a significant anisotropy in their individual compressibilities, with b being more compressible than the others. The higher compressibility along b can be rationalized by noting that this direction is parallel to the boron plane and the half-occupied boron chain is also oriented in this direction. The normalized unit cell parameters versus pressure are shown in Figure 9.

The β-modification of Ir_4B_5 was investigated up to a maximum pressure of 40 GPa, also showing no indication for a pressure induced structural phase transition (Figure 9b). The bulk modulus is 249(3) GPa for B_0 (β-Ir_4B_5, third order) with B' = 3.2(3), which is smaller compared to the α-modification. The new modification β-Ir_4B_5, which was synthesized under high pressure conditions, shows a lower bulk modulus than α-Ir_4B_5, which is in conflict with the expected behavior, namely, that high-pressure phases should form more dense structures and are harder to compress. Hence, β-Ir_4B_5 is not a high-pressure modification of α-Ir_4B_5. High-pressure diffraction patterns of the two modifications at similar pressures are shown in Figures 10 and S1.

Ir_5B_4 was investigated up to a maximum pressure of 50 GPa, and there are no indications of a structural phase transition. The bulk modulus is B_0 (Ir_5B_4, third order) = 310(5) GPa with the pressure derivative B' (Ir_5B_4, third order) = 3.7(2). The lattice parameters do not show a significant anisotropy in their compression behavior (Figure S2).

We further investigated both modifications of Ir_4B_{3-x} up to a maximum pressure of 33 GPa. We investigated a mixture of both modifications in one experiment in the same DAC at exactly the same pressure points. By scanning the sample with a high resolution (2 × 2 μm^2) grid, we found spots, where either orthorhombic Ir_4B_{3-x} or hexagonal Ir_4B_{3-x} were present as the main phase, along with unreacted iridium and the respective other polymorph. The bulk modulus of the orthorhombic modification from fitting a third-order BM

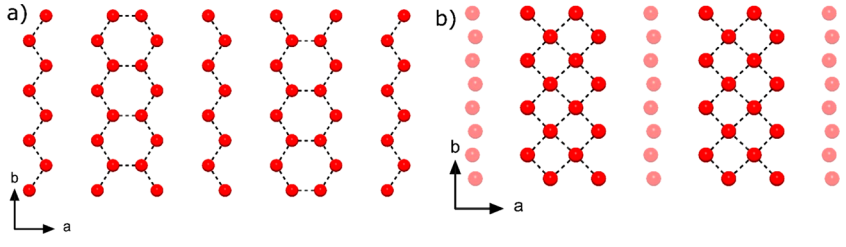

Figure 8. (a) Double and single boron zigzag chains in V_5B_6.[68] (b) For comparison, double and single boron chains in β-Ir_4B_5.

DOI: 10.1021/acs.inorgchem.8b01541
Inorg. Chem. 2018, 57, 10341−10351

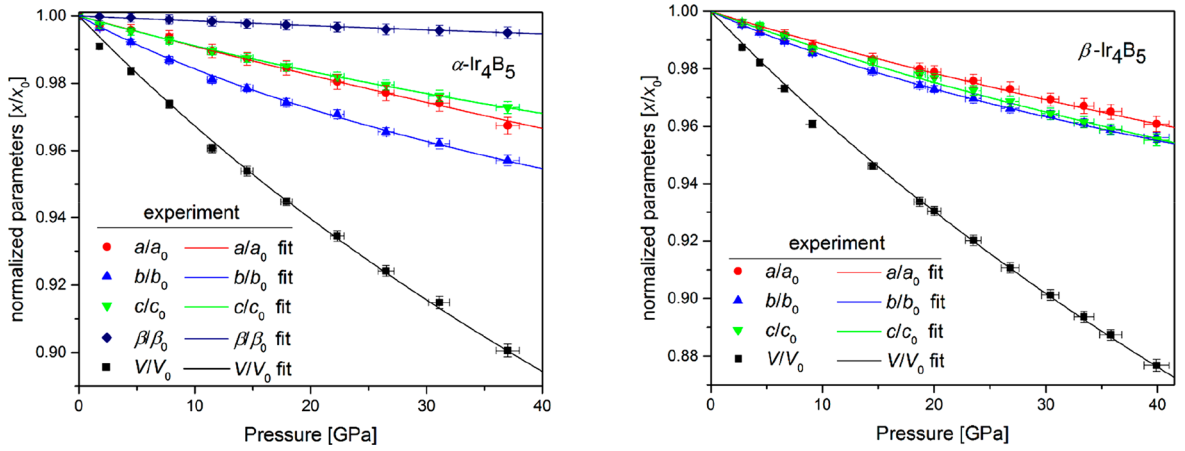

Figure 9. Compression behavior of the normalized unit cell parameters of α-Ir_4B_5 up to 38 GPa (left) and β-Ir_4B_5 up to 40 GPa (right).

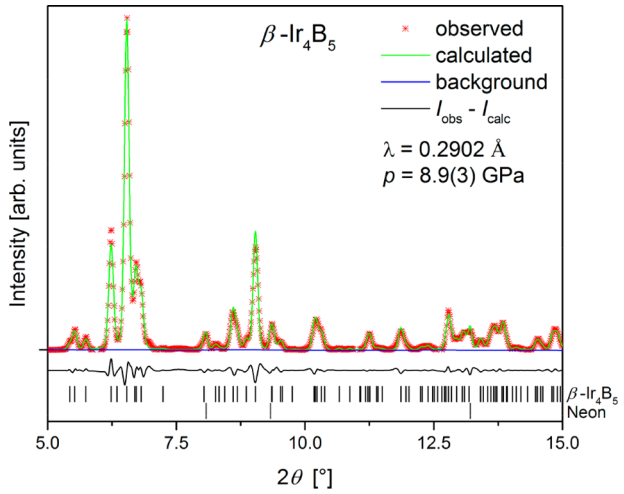

Figure 10. Le Bail refinement of β-Ir_4B_5 at 8.9(3) GPa. The experimental powder diffraction pattern is shown in red, the background is shown in blue, the calculated pattern is shown in green, and the difference plot is shown in black.

Table 4. Experimental and Calculated Results of the Compressibility[a]

compound	space group	BM order	B_0 (GPa) (exp)	B'
α-Ir_4B_5	$C2/m$	2nd	292(5)	4
		3rd	280(6)	4.4(3)
		DFT	225(1)	
β-Ir_4B_5	$Pnma$	2nd	239(3)	4
		3rd	249(3)	3.2(3)
		DFT	265(1)	
Ir_5B_4	$I4_1/a$	2nd	304(6)	4
		3rd	310(5)	3.7(2)
		DFT	287(1)	
orthorhombic Ir_4B_{3-x}	$Cmc2_1$	2nd	336(8)	4
		3rd	320(6)	5.5(4)
		DFT	*b*	
hexagonal Ir_4B_{3-x}	$P\bar{6}m2$	2nd	293(4)	4
		3rd	279(4)	5.2(4)
		DFT	*b*	
Ir	$Fm\bar{3}m$	2nd	341(5)	4
		3rd	326(3)	5.3(2)
		DFT	346(1)	

[a]The DFT values were obtained from stress−strain relations. [b]Due to the partial occupation of some boron positions in the orthorhombic and hexagonal Ir_4B_{3-x} phases, no appropriate model calculation could be carried out.

EOS is 320(6) GPa for B_0 (orthorhombic Ir_4B_{3-x}, third order) with B' = 5.2(4). The compression behavior of the lattice parameters shows no anisotropy. Hexagonal Ir_4B_{3-x} shows a higher compressibility with B_0 (hexagonal Ir_4B_{3-x}, third order) = 279(4) GPa and B' = 5.2(4) for the third-order fit. The compression behavior of the lattice parameters shows a slight anisotropy.

To obtain a better understanding of the changes introduced by the incorporation of boron into the structures, we collected pressure data of elemental iridium up to a pressure of 50 GPa. We found a bulk modulus of B_0 (Ir, third order) = 326(3) GPa with B' = 5.3(2). A summary of the compressibilities of all phases is given in Table 4. The compression behavior showing the third-order fits is displayed in Figures 9 and S2−S5, and the pressure dependence of the unit cell parameters is listed in Tables S2−S6.

The incorporation of boron into the structures does not enhance the incompressibility but leads to a significant reduction of the bulk modulus in comparison to elemental iridium. This is in contrast to the observations on rhenium or osmium borides, where the incorporation of boron leads to a decrease of the compressibility with respect to the compressibility of the elements.[5,70−72] The investigated phases however follow the trend to become more compressible as the amount of boron in the structures increases. Orthorhombic Ir_4B_{3-x}, being the most metal-rich phase, almost reaches the bulk modulus of elemental iridium. The new phase β-Ir_4B_5 on the other hand shows a compressibility which is approaching the rather low value of 224(15) GPa of elemental boron.[73] The findings in this study thus support the statement of Gu et al., who correlated an increasing amount of boron in borides with a decreasing bulk modulus.[5]

Hardness. The hardness of β-Ir_4B_5 was obtained at different indentation loads in order to allow an extrapolation of the load dependence and in order to enable a comparison to data from earlier studies. The asymptotic response of the material's hardness to increasing loads is depicted in Figure 11. In the load regime between 9.8 and 2.94 N, the hardness remains almost constant, showing a hardness of approximately 16 GPa. At lower forces, the hardness increases to a maximum value of H_V (0.49 N, β-Ir_4B_5) = 22.6(2.8) GPa at 0.49 N. The

DOI: 10.1021/acs.inorgchem.8b01541
Inorg. Chem. 2018, 57, 10341−10351

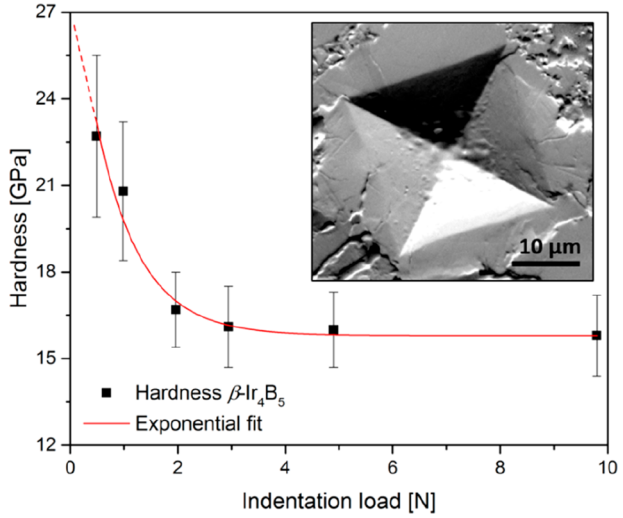

Figure 11. Load-dependent hardness of β-Ir_4B_5. The data were fitted with an exponential to extrapolate the material hardness at infinitesimal loads. The extrapolation of the fit is indicated by a dashed line.

hardness of β-Ir_4B_5, which ranges from H_V (9.8 N, β-Ir_4B_5) = 15.8(1.2) GPa to H_V (0.49 N, β-Ir_4B_5) = 22.6(2.8) GPa, is significantly lower than the values reported for the α-modification (49.8 at 0.49 N and 18.2 GPa at 9.8 N), or Ir_5B_4 (43 GPa).[3,30] However, the hardness data for α-Ir_4B_5 and Ir_5B_4 were obtained using very thin films consisting of nm-sized crystals on a substrate of different chemical constitution (TiB_2/BN composite) which might have resulted in significant overestimation of the values. Furthermore, the XRD pattern of Ir_5B_4 in the study of Latini et al. (2010) showed indications of an impurity phase which formed during the laser deposition experiments. In contrast, our results are in good agreement with the observation of Samsonov et al. on bulk samples, who found a hardness of only 15.8(8) GPa for Ir_5B_4.[74] Therefore, we conclude that the bulk hardness of iridium boride phases is not as high as previously assumed on the basis of thin film measurements.

Microcalorimetry. Microcalorimetry was performed on polycrystalline samples of α-Ir_4B_5 and β-Ir_4B_5, which weighed between 20 and 25 mg. The comparison of the heat capacity curves for both modifications can be seen in Figure S6. Both curves show no peaks at low temperatures, and hence, there seems to be no transition into a superconducting state down to 2 K. There is excellent agreement for the ambient temperature values of the heat capacity, enthalpy, and entropy with published data for elemental boron and iridium. The Debye temperature of β-Ir_4B_5 (444(4) K) is higher than the temperature of α-Ir_4B_5 (392(4) K), whereas both are in the same temperature range as elemental iridium (420 K) and noticeably smaller than the Debye temperature of elemental boron (1219 K). The herein determined values for the Debye temperature of elemental iridium (343(3) K) and boron (928(9) K) are smaller than the values tabulated in the literature.[75,76] These deviations can arise from different fitting ranges and fitting difficulties. The T^3-plots are shown in Figures S7–S10. All derived thermodynamic values, including those of elemental boron and iridium, are listed in Table 5.

DFT Calculations. DFT calculations were performed on simplified model structures. We disregarded occupational disorder in the structures and assumed full site occupancies for each phase. These simplifications turned out to be inappropriate for both Ir_4B_{3-x} modifications, and therefore, no further calculations were carried out for this composition. Ir_5B_4 was approximated by $Ir_{20}B_{16}$, α-Ir_4B_5 by $C2/m$-Ir_8B_{12} with a full occupation of the Wyckoff position 4*i*, and β-Ir_4B_5 by *Pnma*-Ir_8B_{12}. Stress–strain calculations allowed us to obtain the elastic stiffness coefficients c_{ij}, bulk modulus B, shear modulus G, Young's modulus Y, Poisson's ratio υ, Debye temperature Θ_D, universal anisotropy index A_U, and hardness H (Table 6). The calculated Debye temperatures for α-Ir_4B_5

Table 6. Elastic Properties from the Elastic DFT-GGA Calculations

	*C*2/*m* - "Ir_8B_{12}"	*Pnma* - "Ir_8B_{12}"	"$Ir_{20}B_{16}$"	
	α-Ir_4B_5	β-Ir_4B_5	Ir_5B_4	Ir
c_{11} (GPa)	373(3)	482(4)	494(2)	583(1)
c_{22} (GPa)	303(3)	390(1)		
c_{33} (GPa)	303(2)	433(4)	460(2)	
c_{44} (GPa)	50(1)	112(1)	72(1)	256(1)
c_{55} (GPa)	125(1)	102(2)		
c_{66} (GPa)	58(1)	60(1)	162(1)	
c_{12} (GPa)	150(2)	170(2)	221(2)	228(1)
c_{13} (GPa)	160(2)	122(2)	177(1)	
c_{15} (GPa)	58(1)			
c_{16} (GPa)			40(1)	
c_{23} (GPa)	217(2)	250(2)		
c_{25} (GPa)	−32(1)			
c_{35} (GPa)	7(1)			
c_{46} (GPa)	−29(1)			
B_{cij} (GPa)	225(1)	265(1)	287(1)	346(1)
G_{cij}[a] (GPa)	63(8)	99(5)	110(6)	222(2)
Y_{cij} (GPa)	180(10)	266(10)	295(15)	550(5)
υ_{cij}	0.37(1)	0.33(1)	0.33(1)	0.23
Θ_D (K)	324(2)	414(2)	382(2)	428(3)
A_U[b]	2.5(1)	0.7	0.9(1)	0.16(1)
H (GPa)	4.5(5)	8.5(5)	9(1)	25(1)

[a] $2G(1+\upsilon) = Y = 3B(1-2\upsilon)$ for isotropic materials. [b] $A_U = 5G^V/G^R + B^V/B^R - 6 \geq 0$ (G^V and G^R Voigt and Reuss estimates of G, B^V and B^R = Voigt and Reuss estimates of B).[77]

Table 5. Thermodynamical Properties of α-Ir_4B_5, β-Ir_4B_5, Elemental Ir, and Elemental B at 298 K

compound	C_P (J/mol K)	H^0_{298} (J/mol)	S^0_{298} (J/mol K)	Θ_D (K)	reference
α-Ir_4B_5	291(1)	39770(700)	227(2)	392(4)	this study
β-Ir_4B_5	223(1)	32930(600)	191(1)	444(4)	this study
Ir elemental	24.8(2)	5232(50)	35.3(3)	343(3)	this study
Ir elemental	25.09	5266	35.49	420	Arblaster[76]
B elemental	11.2(1)	1220(15)	5.93(9)	928(9)	this study
B elemental	11.1(1)	1222(8)	5.90(8)	1219	Thompson and McDonald[75]

DOI: 10.1021/acs.inorgchem.8b01541
Inorg. Chem. 2018, 57, 10341–10351

(324(2) K) and β-Ir_4B_5 (414(2) K) are in moderate agreement with the experimental values (392(4) K for α-Ir_4B_5 and 444(4) K for β-Ir_4B_5). The Debye temperature for elemental iridium (428(3) K) is in excellent agreement with the value from the literature (420 K).[76] The calculated bulk moduli of the three phases are similar to the values obtained by the experimental measurements (Table 4). This justifies to some extent the neglect of the partial occupation but, conversely, also indicates that a minor change in the boron content will not influence the physical properties significantly. The values of the calculated and measured hardness however differ considerably for the phases. These deviations can be explained by the fact that the hardness of a material is primarily a surface property and the calculations are volume-based parameters.

CONCLUSIONS

We report the successful synthesis of β-Ir_4B_5, the first 5*d* transition metal boride synthesized under high-pressure conditions, as well as the synthesis and characterization of the binary iridium borides orthorhombic Ir_4B_{3-x}, hexagonal Ir_4B_{3-x}, Ir_5B_4, and α-Ir_4B_5. The structure of the new modification was solved unambiguously by combining single-crystal XRD and complementing neutron diffraction experiments to unequivocally locate the boron atoms and determine their site occupancies. There are some similarities between the structures of β-Ir_4B_5 with both α-Ir_4B_5 and the V_5B_6-structure type; however, the alignment of the double boron chains in combination with the half-occupied single chain in β-Ir_4B_5 is unique and therefore constitutes a new structure type. Even though the synthesis of β-Ir_4B_5 was carried out under high-pressure/high-temperature conditions, our findings (compressibility, unit cell volume, microcalorimetry) clearly show that it is not a high-pressure polymorph of Ir_4B_5. The structure was not among the numerous predicted possible structures. By using microcalorimetry measurements, the heat capacities of α-Ir_4B_5 and β-Ir_4B_5 were determined. Both phases do not seem to become superconducting at low temperatures. The hardness measurements revealed a significantly lower hardness for bulk β-Ir_4B_5 than Latini et al. found for thin films of α-Ir_4B_5.[30] As the crystal structure and composition for both modifications are similar, the huge difference in the hardness value presumably arises from other reasons. We conclude that the hardness of α-Ir_4B_5 is either not as high as previously assumed on the basis of thin films measurements or that such observations are at least not extendable to bulk properties. The values for the bulk moduli B_0 of the iridium borides vary between 249(3) and 320(6) GPa (third-order BM fits). Iridium borides do not reach the ultra-incompressibility of diamond (443 GPa) and OsB (431−453 GPa), or other incompressible period-6 transition metal borides.[5,71] The incorporation of boron into the structures does not enhance the compressibility but leads to a significant reduction of the bulk modulus in comparison to elemental iridium (B_0, third order = 326(3) GPa). These findings for iridium borides are in contrast to the observations on rhenium or osmium borides, where the incorporation of boron leads to a decrease of the compressibility with respect to the compressibility of the elements.[5,70−72] Thus, ongoing research in the field of binary borides is crucial for a better understanding of the exact influence of boron incorporation into heavy transition metals.

ASSOCIATED CONTENT

Supporting Information

The Supporting Information is available free of charge on the ACS Publications website at DOI: 10.1021/acs.inorgchem.8b01541.

Detailled description of the derivation for the compressibility and microcalorimetry, crystallographic data collected by neutron and X-ray diffraction, X-ray powder pattern of β- and α-Ir_4B_5 at 7.8(3) GPa, compression behavior of β-Ir_4B_5, α-Ir_4B_5, Ir_5B_4, orthorhombic Ir_4B_{3-x}, and hexagonal Ir_4B_{3-x}, heat capacity of α-Ir_4B_5 and β-Ir_4B_5, and Debye temperature of α-Ir_4B_5, β-Ir_4B_5, elemental iridium, and elemental boron (PDF)

Accession Codes

CCDC 1847116 contains the supplementary crystallographic data for this paper. These data can be obtained free of charge via www.ccdc.cam.ac.uk/data_request/cif, or by emailing data_request@ccdc.cam.ac.uk, or by contacting The Cambridge Crystallographic Data Centre, 12 Union Road, Cambridge CB2 1EZ, UK; fax: +44 1223 336033.

AUTHOR INFORMATION

Corresponding Author

*E-mail: Hubert.Huppertz@uibk.ac.at. Fax: +43 (512) 507-57099.

ORCID

Hubert Huppertz: 0000-0002-2098-6087

Author Contributions

All authors have given approval to the final version of the manuscript

Notes

The authors declare no competing financial interest.

ACKNOWLEDGMENTS

The authors thank Dominik Spahr and Chris-Julian Fruhner for their support and help during beamtimes at P02.2/PETRA III. We thank Dr. Anatoliy Senyshyn (Forschungsneutronenquelle FRM II, Heinz Maier-Leibnitz, Technische Universität München, Garching, Deutschland) for the help with the neutron diffraction measurements. We gratefully acknowledge the DFG (project 1232-401-1) and the FWF (I-1636-N19) for funding in the framework of an ERA-chemistry project. Furthermore, we thank the BMBF (project 05K13RF1 and 05K16RFB) and the Conacyt grant (FC-2015-2-947) for funding. The Hermann Willkomm-Stiftung in Frankfurt is also acknowledged for providing travel grants.

REFERENCES

(1) Chung, H.-Y.; Weinberger, M. B.; Levine, J. B.; Kavner, A.; Yang, J.-M.; Tolbert, S. H.; Kaner, R. B. Synthesis of ultra-incompressible superhard rhenium diboride at ambient pressure. *Science* **2007**, *316*, 436−439.

(2) Gou, H.; Dubrovinskaia, N.; Bykova, E.; Tsirlin, A. A.; Kasinathan, D.; Schnelle, W.; Richter, A.; Merlini, M.; Hanfland, M.; Abakumov, A. M. Discovery of a superhard iron tetraboride superconductor. *Phys. Rev. Lett.* **2013**, *111*, 157002.

(3) Rau, J.; Latini, A. New hard and superhard materials: $RhB_{1.1}$ and $IrB_{1.35}$. *Chem. Mater.* **2009**, *21*, 1407−1409.

(4) Mohammadi, R.; Lech, A. T.; Xie, M.; Weaver, B. E.; Yeung, M. T.; Tolbert, S. H.; Kaner, R. B. Tungsten tetraboride, an inexpensive superhard material. *Proc. Natl. Acad. Sci. U. S. A.* **2011**, *108*, 10958−62.

DOI: 10.1021/acs.inorgchem.8b01541
Inorg. Chem. 2018, 57, 10341−10351

(5) Gu, Q.; Krauss, G.; Steurer, W. Transition Metal Borides: Superhard versus Ultra-incompressible. *Adv. Mater.* **2008**, *20*, 3620−3626.
(6) Nagamatsu, J.; Nakagawa, N.; Muranaka, T.; Zenitani, Y.; Akimitsu, J. Superconductivity at 39 K in magnesium diboride. *Nature* **2001**, *410*, 63−64.
(7) Xie, W.; Luo, H.; Baroudi, K.; Krizan, J. W.; Phelan, B. F.; Cava, R. J. Fragment-based design of NbRuB as a new metal-rich boride superconductor. *Chem. Mater.* **2015**, *27*, 1149−1152.
(8) Economy, J.; Lin, R.; Matkovich, V. *Boron and Refractory Borides*; Springer-Verlag: Berlin, 1977.
(9) Albert, B.; Hillebrecht, H. Boron: elementary challenge for experimenters and theoreticians. *Angew. Chem., Int. Ed.* **2009**, *48*, 8640−8668.
(10) Zeiringer, I.; Cheng, X.; Chen, X.-Q.; Bauer, E.; Giester, G.; Rogl, P. F. Crystal structures and constitution of the binary system iridium-boron. *Sci. China. Mater.* **2015**, *58*, 649−668.
(11) Zhao, X.; Nguyen, M. C.; Wang, C.-Z.; Ho, K.-M. New stable Re−B phases for ultra-hard materials. *J. Phys.: Condens. Matter* **2014**, *26*, 455401.
(12) Wei, S.; Li, D.; Lv, Y.; Liu, Z.; Xu, C.; Tian, F.; Duan, D.; Liu, B.; Cui, T. Ground State Structures of Tantalum Tetraboride and Triboride: an ab initio Study. *Phys. Chem. Chem. Phys.* **2016**, *18*, 18074−18080.
(13) Li, X.; Wang, H.; Lv, J.; Liu, Z. Phase diagram and physical properties of iridium tetraboride from first principles. *Phys. Chem. Chem. Phys.* **2016**, *18*, 12569−12575.
(14) Chu, B.; Li, D.; Bao, K.; Tian, F.; Duan, D.; Sha, X.; Hou, P.; Liu, Y.; Zhang, H.; Liu, B. The crystal structure of IrB_2: a first-principle calculation. *RSC Adv.* **2014**, *4*, 63442−63446.
(15) Kolmogorov, A.; Shah, S.; Margine, E.; Bialon, A.; Hammerschmidt, T.; Drautz, R. New superconducting and semiconducting Fe-B compounds predicted with an ab initio evolutionary search. *Phys. Rev. Lett.* **2010**, *105*, 217003.
(16) Bialon, A.; Hammerschmidt, T.; Drautz, R.; Shah, S.; Margine, E.; Kolmogorov, A. Possible routes for synthesis of new boron-rich Fe−B and $Fe_{1-x}Cr_xB_4$ compounds. *Appl. Phys. Lett.* **2011**, *98*, No. 081901.
(17) Bykova, E.; Gou, H.; Bykov, M.; Hanfland, M.; Dubrovinsky, L.; Dubrovinskaia, N. Crystal structures and compressibility of novel iron borides Fe_2B_7 and Fe_xB_{50} synthesized at high pressure and high temperature. *J. Solid State Chem.* **2015**, *230*, 102−109.
(18) Gou, H.; Tsirlin, A. A.; Bykova, E.; Abakumov, A. M.; Van Tendeloo, G.; Richter, A.; Ovsyannikov, S. V.; Kurnosov, A. V.; Trots, D. M.; Konôpková, Z. Peierls distortion, magnetism, and high hardness of manganese tetraboride. *Phys. Rev. B: Condens. Matter Mater. Phys.* **2014**, *89*, No. 064108.
(19) Bykova, E.; Tsirlin, A. A.; Gou, H.; Dubrovinsky, L.; Dubrovinskaia, N. Novel non-magnetic hard boride Co_5B_{16} synthesized under high pressure. *J. Alloys Compd.* **2014**, *608*, 69−72.
(20) Wang, S.; Yu, X.; Zhang, J.; Zhang, Y.; Wang, L.; Leinenweber, K.; Xu, H.; Popov, D.; Park, C.; Yang, W. Crystal structures, elastic properties, and hardness of high-pressure synthesized CrB_2 and CrB_4. *J. Superhard Mater.* **2014**, *36*, 279−287.
(21) Knappschneider, A.; Litterscheid, C.; Kurzman, J.; Seshadri, R.; Albert, B. Crystal structure refinement and bonding patterns of CrB_4: A boron-rich boride with a framework of tetrahedrally coordinated B atoms. *Inorg. Chem.* **2011**, *50*, 10540−10542.
(22) Knappschneider, A.; Litterscheid, C.; Dzivenko, D.; Kurzman, J. A.; Seshadri, R.; Wagner, N.; Beck, J.; Riedel, R.; Albert, B. Possible superhardness of CrB_4. *Inorg. Chem.* **2013**, *52*, 540−542.
(23) Knappschneider, A.; Litterscheid, C.; George, N. C.; Brgoch, J.; Wagner, N.; Beck, J.; Kurzman, J. A.; Seshadri, R.; Albert, B. Peierls-Distorted Monoclinic MnB_4 with a Mn-Mn Bond. *Angew. Chem., Int. Ed.* **2014**, *53*, 1684−1688.
(24) Knappschneider, A.; Litterscheid, C.; Brgoch, J.; George, N. C.; Henke, S.; Cheetham, A. K.; Hu, J. G.; Seshadri, R.; Albert, B. Manganese Tetraboride, MnB_4: High-Temperature Crystal Structure, p−n Transition, ^{55}Mn NMR Spectroscopy, Solid Solutions, and Mechanical Properties. *Chem. - Eur. J.* **2015**, *21*, 8177−8181.
(25) Aronsson, B.; Stenberg, E.; Aselius, J. Borides of rhenium and the platinium metals - the crystal structure of Re_7B_3, ReB_3, Rh_7B_3, $RhB_{1.1}$, $IrB_{1.1}$ and PtB. *Acta Chem. Scand.* **1960**, *14*, 733−741.
(26) Aronsson, B.; Stenberg, E.; Åselius, J. Borides of ruthenium, osmium and iridium. *Nature* **1962**, *195*, 377−378.
(27) Aronsson, B. The Crystal Structure of RuB_2, OsB_2 and $IrB_{1.35}$ and Some General Comments on the Crystal Chemistry of Borides in the Composition Range MeB-MeB_3. *Acta Chem. Scand.* **1963**, *17*, 2036−2050.
(28) Rogl, P.; Nowotny, H.; Benesovsky, F. Ein Beitrag zur Strukturchemie der Iridiumboride. *Monatsh. Chem.* **1971**, *102*, 678−686.
(29) Xie, Z.; Blair, R. G.; Orlovskaya, N.; Cullen, D. A.; Lapidus, S. H.; Kata, D.; Rutkowski, P.; Lis, J. In search of the elusive IrB_2: Can mechanochemistry help? *J. Solid State Chem.* **2016**, *233*, 108−119.
(30) Latini, A.; Rau, J. V.; Teghil, R.; Generosi, A.; Albertini, V. R. Superhard properties of rhodium and iridium boride films. *ACS Appl. Mater. Interfaces* **2010**, *2*, 581−587.
(31) Ivanovskii, A. Mechanical and electronic properties of diborides of transition 3d−5d metals from first principles: Toward search of novel ultra-incompressible and superhard materials. *Prog. Mater. Sci.* **2012**, *57*, 184−228.
(32) Wang, D. Y.; Wang, B.; Wang, Y. X. New crystal structures of IrB and IrB_2: first-principles calculations. *J. Phys. Chem. C* **2012**, *116*, 21961−21966.
(33) Wang, Y.; Wu, L.; Lin, Y.; Hu, Q.; Li, Z.; Liu, H.; Zhang, Y.; Gou, H.; Yao, Y.; Zhang, J. Structures and stability of novel transition-metal (M= Co, Rh, Co and Ir) borides. *Phys. Rev. B: Condens. Matter Mater. Phys.* **2015**, *92*, 174106.
(34) Yan, Q.; Wang, Y. X.; Wang, B.; Yang, J.; Yang, G. The ground-state structure and physical properties of ReB_3 and IrB_3 predicted from first principles. *RSC Adv.* **2015**, *5*, 25919−25928.
(35) Huppertz, H. Multianvil high-pressure/high-temperature synthesis in solid state chemistry. *Z. Kristallogr. - Cryst. Mater.* **2004**, *219*, 330−338.
(36) Walker, D.; Carpenter, M.; Hitch, C. Some simplifications to multianvil devices for high pressure experiments. *Am. Mineral.* **1990**, *75*, 1020−1028.
(37) Bruker, A. TOPAS V3: General profile and structure analysis software for powder diffraction data. User's Manual, Bruker AXS, Karlsruhe, Germany, 2005.
(38) Sheldrick, G. *Sadabs-2014*, 5; Bruker Analytical X-ray Instruments Inc: Madison, WI, 2015.
(39) Sheldrick, G. *SHELXS-13 and SHELXL-13*; University of Göttingen: Göttingen, Germany, 2013.
(40) Sheldrick, G. M. Crystal structure refinement with SHELXL. *Acta Crystallogr., Sect. C: Struct. Chem.* **2015**, *71*, 3−8.
(41) Spek, A. Single-crystal structure validation with the program PLATON. *J. Appl. Crystallogr.* **2003**, *36*, 7−13.
(42) Brandenburg, K.; Putz, H. *Diamond−Crystal and Molecular Structure Visualization*; Crystal Impact: Bonn, Germany, 2012.
(43) Hoelzel, M.; Senyshyn, A.; Juenke, N.; Boysen, H.; Schmahl, W.; Fuess, H. High-resolution neutron powder diffractometer SPODI at research reactor FRM II. *Nucl. Instrum. Methods Phys. Res., Sect. A* **2012**, *667*, 32−37.
(44) Hoelzel, M.; Senyshyn, A.; Dolotko, O. SPODI: High resolution powder diffractometer. *JLSRF* **2015**, *1*, DOI: 10.17815/jlsrf-1-24.
(45) Sears, V. F. Neutron scattering lengths and cross sections. *Neutron news* **1992**, *3*, 26−37.
(46) National Institute of Standards and Technology - Center for Neutron Research. www.ncnr.nist.gov (Oct 24, 2017).
(47) Boehler, R. New diamond cell for single-crystal x-ray diffraction. *Rev. Sci. Instrum.* **2006**, *77*, 115103.
(48) Mao, H. K.; Bell, P. M.; Shaner, J. W.; Steinberg, D. J. Specific volume measurements of Cu, Mo, Pd, and Ag and calibration of the

DOI: 10.1021/acs.inorgchem.8b01541
Inorg. Chem. 2018, 57, 10341−10351

ruby R_1 fluorescence pressure gauge from 0.06 to 1 Mbar. *J. Appl. Phys.* **1978**, *49*, 3276−3283.
(49) Liermann, H.-P.; Konôpková, Z.; Morgenroth, W.; Glazyrin, K.; Bednarčik, J.; McBride, E.; Petitgirard, S.; Delitz, J.; Wendt, M.; Bican, Y. The extreme conditions beamline P02.2 and the extreme conditions science infrastructure at PETRA III. *J. Synchrotron Radiat.* **2015**, *22*, 908−924.
(50) Hammersley, A. FIT2D: an introduction and overview. *European Synchrotron Radiation Facility Internal Report ESRF97-HA02T* **1997**, *68*, 58.
(51) Prescher, C.; Prakapenka, V. B. DIOPTAS: a program for reduction of two-dimensional X-ray diffraction data and data exploration. *High Pressure Res.* **2015**, *35*, 223−230.
(52) Murnaghan, F. The compressibility of media under extreme pressures. *Proc. Natl. Acad. Sci. U. S. A.* **1944**, *30*, 244−247.
(53) Birch, F. Finite elastic strain of cubic crystals. *Phys. Rev.* **1947**, *71*, 809.
(54) Angel, R. J.; Alvaro, M.; Gonzalez-Platas, J. EosFit7c and a Fortran module (library) for equation of state calculations. *Z. Kristallogr. - Cryst. Mater.* **2014**, *229*, 405−419.
(55) Lashley, J.; Hundley, M.; Migliori, A.; Sarrao, J.; Pagliuso, P.; Darling, T.; Jaime, M.; Cooley, J.; Hults, W.; Morales, L. Critical examination of heat capacity measurements made on a Quantum Design physical property measurement system. *Cryogenics* **2003**, *43*, 369−378.
(56) Quantum Design, San Diego, CA.
(57) Carslaw, H.; Jaeger, J. *Heat in Solids*; Clarendon Press, Oxford: 1959; Vol. *1*.
(58) Clark, S. J.; Segall, M. D.; Pickard, C. J.; Hasnip, P. J.; Probert, M. I.; Refson, K.; Payne, M. C. First principles methods using CASTEP. *Z. Kristallogr. - Cryst. Mater.* **2005**, *220*, 567−570.
(59) Wu, Z.; Cohen, R. E. More accurate generalized gradient approximation for solids. *Phys. Rev. B: Condens. Matter Mater. Phys.* **2006**, *73*, 235116.
(60) Lundstrom, T.; Tergenius, L.-E. Refinement of the Crystal Structure of the Non-stoichiometric Boride $IrB_{1.35}$. *Acta Chem. Scand.* **1973**, *27*, 3705−3711.
(61) Holleman, A. F.; Wiberg, E.; Wiberg, N. *Lehrbuch der Anorganischen Chemie*; Walter de Gruyter-Verlag: Berlin, 2007.
(62) Singh, H. Determination of thermal expansion of germanium, rhodium and iridium by X-rays. *Acta Crystallogr., Sect. A: Cryst. Phys., Diffr., Theor. Gen. Crystallogr.* **1968**, *24*, 469−471.
(63) Aronsson, B. The crystal structure of Ru_7B_3. *Acta Chem. Scand.* **1959**, *13*, 109−114.
(64) Hofmann, K.; Kalyon, N.; Kapfenberger, C.; Lamontagne, L.; Zarrini, S.; Berger, R.; Seshadri, R.; Albert, B. Metastable Ni_7B_3: A New Paramagnetic Boride from Solution Chemistry, Its Crystal Structure and Magnetic Properties. *Inorg. Chem.* **2015**, *54*, 10873−10877.
(65) Hofmann, W.; Jäniche, W. Der Strukturtyp von Aluminiumborid (AlB_2). *Naturwissenschaften* **1935**, *23*, 851−851.
(66) Kiessling, R. The binary system chromium-boron. *Acta Chem. Scand.* **1949**, *3*, 595−602.
(67) La Placa, S.; Post, B. The crystal structure of rhenium diboride. *Acta Crystallogr.* **1962**, *15*, 97−99.
(68) Bolmgren, H.; Lundström, T.; Tergenius, L.-E.; Okada, S.; Higashi, I. The crystal structure of Ta_5B_6. *J. Less-Common Met.* **1990**, *161*, 341−345.
(69) Spear, K.; Gilles, P. Phase and structure relationships in the vanadium-boron system. *High Temp. Sci.* **1969**, *1*, 86−97.
(70) Friedrich, A.; Winkler, B.; Juarez-Arellano, E. A.; Bayarjargal, L. Synthesis of binary transition metal nitrides, carbides and borides from the elements in the laser-heated diamond anvil cell and their structure-property relations. *Materials* **2011**, *4*, 1648−1692.
(71) Neun, C.; Petermüller, B.; Bayarjargal, L.; Morgenroth, W.; Silva-Pereyra, H. G.; Avalos-Borja, M.; Spahr, D.; Schmuck, F.; Milman, V.; Huppertz, H.; Winkler, B. Compressibility, microcalorimetry, elastic properties and EELS of rhenium borides. *Solid State Sci.* **2018**, *81*, 71−81.
(72) Cumberland, R. W.; Weinberger, M. B.; Gilman, J. J.; Clark, S. M.; Tolbert, S. H.; Kaner, R. B. Osmium diboride, an ultra-incompressible, hard material. *J. Am. Chem. Soc.* **2005**, *127*, 7264−7265.
(73) Nelmes, R.; Loveday, J.; Allan, D.; Besson, J.; Hamel, G.; Grima, P.; Hull, S. Neutron-and x-ray-diffraction measurements of the bulk modulus of boron. *Phys. Rev. B: Condens. Matter Mater. Phys.* **1993**, *47*, 7668.
(74) Samsonov, G.; Kosenko, V.; Rud, B.; Sidorova, V. Conditions for the production of Iridium Boride and some of its properties. *Inorg. Mater.* **1972**, *8*, 771−772.
(75) Thompson, J.; McDonald, W. Low-Temperature Thermal Conductivity of Boron. *Phys. Rev.* **1963**, *132*, 82.
(76) Arblaster, J. Thermodynamic properties of the platinum metals on ITS-90. *Platinum Met. Rev.* **1996**, *40*, 62−63.
(77) Ranganathan, S. I.; Ostoja-Starzewski, M. Universal elastic anisotropy index. *Phys. Rev. Lett.* **2008**, *101*, No. 055504.

DOI: 10.1021/acs.inorgchem.8b01541
Inorg. Chem. 2018, 57, 10341−10351